The recoiling of liquid droplets upon collision with solid surfaces

H.-Y. Kim[a] and J.-H. Chun
Department of Mechanical Engineering, Massachusetts Institute of Technology, Cambridge, Massachusetts 02139

(Received 1 March 2000; accepted 5 December 2000)

Although the spreading behavior of liquid droplets impacting on solid surfaces has been extensively studied, the mechanism of recoiling which takes place after the droplet reaches its maximum spread diameter has not yet been fully understood. This paper reports the study of the recoiling behavior of different liquid droplets (water, ink, and silicone oil) on different solid surfaces (polycarbonate and silicon oxide). The droplet dynamics are experimentally studied using a high speed video system. Analytical methods using the variational principle, which were originated by Kendall and Rohsenow (MIT Technical Report 85694-100, 1978) and Bechtel *et al.* [IBM J. Res. Dev. **25**, 963 (1981)], are modified to account for wetting and viscous effects. In our model, an empirically determined dissipation factor is used to estimate the viscous friction. It is shown that the model closely predicts the experimental results obtained for the varying dynamic impact conditions and wetting characteristics. This study shows that droplets recoil fast and vigorously when the Ohnesorge number decreases or the Weber number increases. Droplets with a large equilibrium contact angle are also found to recoil faster. Here the Ohnesorge number scales the resisting force to the recoiling motion, and is shown to play the most important role in characterizing the recoiling motion. [DOI: 10.1063/1.1344183]

I. INTRODUCTION

A liquid droplet impacting with a solid surface will oscillate on the surface unless it possesses negligible impact inertia, splatters, or rapidly freezes. The oscillation of the droplet consists of the initial spreading of the droplet until it reaches its maximum base diameter and subsequent oscillatory motions of recoiling and weak re-spreading. The dynamics of liquid droplets colliding with solid surfaces have been extensively studied for more than a century.[1,2] However, the majority of this effort has been focused on the initial spreading process, i.e., from the moment of impact to the moment when the droplet reaches its maximum base diameter.[3–11] As a result, understanding of the dynamics of the recoiling appears to be very far from complete. This paper reports the study of the recoiling behavior of different liquid droplets (water, ink, and silicone oil) on different solid surfaces (polycarbonate and silicon oxide).

Although the ''mechanism'' of recoiling has not yet been investigated, there were some authors who reported the oscillatory motions of a droplet upon impact. Elliot and Ford[12] reported that the impacting drop undergoes several stages, including spreading and retraction, before it reaches a sessile drop form. Cheng[13] measured the dampened vibratory motion of water drops impacting onto a coal surface. Fukai *et al.*[14,15] conducted a theoretical study on the spreading and recoiling of a liquid droplet upon collision with a solid surface. Their model was based on solving the full Navier–Stokes equation by utilizing deforming finite elements and allowing the contact line to slip. Their prediction was in a qualitative agreement with the experimental results, but the investigation of the recoiling dynamics itself was not conducted. Pasandideh-Fard *et al.*[16] also performed a numerical study of droplet impact. Their model solved the full Navier–Stokes equation using a modified SOLA–VOF method. SOLA–VOF (SOLution Algorithm–Volume Of Fraction) is a program for the solution of two-dimensional transient fluid flow with free boundaries, based on the concept of a fractional volume of fluid. Their model accurately predicted droplet contact diameters obtained by experimental measurements during the initial spreading stages. However, a discrepancy was revealed during the recoiling stages. Schiaffino and Sonin[17] discussed the oscillations of a droplet's centerline elevation after its footprint is arrested by freezing on a subcooled target of its own kind. They found that the oscillation damping time of a deposited water droplet is in good agreement with the damping time of a negligibly viscous, liquid drop that oscillates freely. Recently, Aziz and Chandra[18] photographed a vigorous recoiling of a molten tin droplet impacting on a heated stainless steel plate.

In this work, we experimentally study the spreading and recoiling of different droplets on different solid surfaces to investigate not only the effects of dynamic impact conditions but also the wetting effects arising from different combinations of liquids and solids. In addition, we present approximate models to predict the behavior of the droplets. Our theoretical study is based on an approach to the dynamics of droplet impact, originated by Kendall and Rohsenow[19] and Bechtel *et al.*[20] The approach utilizes the variational principle rather than the Navier–Stokes equation. Its advantage is that by assuming the geometry of the deforming droplet, a simple differential equation can be obtained to describe the

[a]Author to whom correspondence should be addressed. Present address: Thermal/Flow Control Research Center, Korea Institute of Science and Technology, Seoul 130-650, Korea. Telephone: 82-2-958-6709; Fax: 82-2-958-5689; electronic mail: hoyoung@kist.re.kr

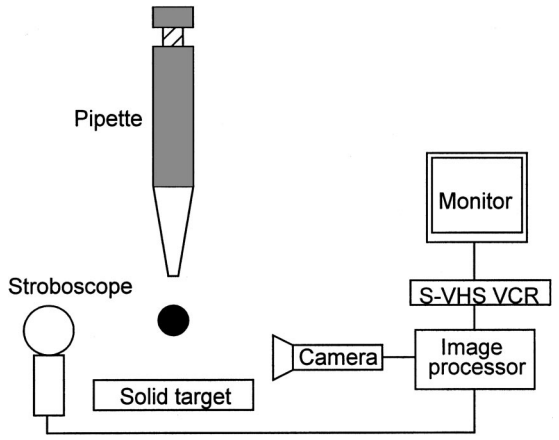

FIG. 1. Experimental apparatus for the high speed imaging of droplet dynamics.

droplet dynamics. Therefore, if the approximate models provide sufficiently accurate predictions, one can save significant computational efforts required to solve the Navier–Stokes equation numerically. Although there exist several simplified models to describe the ''initial spreading'' process by a single equation,[16,21–23] simple modeling for the ''recoiling'' process has been sparse except those of Refs. 19 and 20. Moreover, unlike numerical analysis based on the full Navier–Stokes equation, the models presented here greatly facilitate the analytical study of the recoiling mechanism and the effects of various parameters including inertia and interfacial properties.

First we describe the experimental methods and then present the approximate models of the droplet dynamics. In the models, two different droplet shapes, i.e., a cylinder and a truncated sphere, are assumed and each model is based upon the method of Refs. 19 and 20, respectively. The experimental results are compared with the predictions of our models. Finally, the effects of dynamic impact conditions and wetting characteristics on the recoiling behavior are discussed to elucidate the mechanism underlying the recoiling.

II. DESCRIPTION OF THE EXPERIMENTAL APPARATUS

The experimental apparatus is illustrated in Fig. 1. It consists of a pipette which gently ejects a liquid droplet, a flat target on which the droplet falls, a high-speed video system to record the shape evolution of the droplet, and a stroboscope which is synchronized with the video system. As the experimental liquids, deionized water, ink (NCR 940607), and silicone oil (Dow Corning 704 diffusion pump oil) are used. Table I shows the physical properties of these liquids.

TABLE I. Physical properties of the liquids used in the experiments.

Liquid	Density (kg/m^3)	Surface tension (N/m)	Viscosity (kg/(m s))
Water	996	0.0717	8.67×10^{-4}
Ink	1052	0.055	2.6×10^{-3}
Silicone oil	1064	0.0373	3.63×10^{-2}

TABLE II. Equilibrium contact angles.

Liquid	Solid	Contact angle
Deionized water	Polycarbonate	87.4°
Deionized water	Silicon oxide	58.6°
Ink	Polycarbonate	70.9°
Ink	Silicon oxide	51.5°
Silicone oil	Polycarbonate	6.2°

To examine various impact conditions, the velocity prior to impact is varied by changing the distance between the pipette and the target. In addition, two different sizes of pipettes (Gilson Pipetman P200 and P1000) are used to vary the original droplet diameter.

Since the droplet motions, especially recoiling, are extremely sensitive to the cleanness of target surfaces, the target materials are selected such that the surface contamination due to dusts, oils, etc., is expected to be very low. As a consequence, the compact disc (polycarbonate) and the thermally oxidized silicon wafer (silicon oxide, SiO_2) are selected as the target surfaces. Our experiments revealed that it is very difficult to obtain consistent results (e.g., equilibrium contact angle and recoiling speed) using commercial glass unless it is cleaned with extreme care. The root-mean-square (RMS) surface roughness of polycarbonate surface was measured to be 1.3 nm with 4.8% of standard deviation by scanning areas of $(10\ \mu m)^2$ using an atomic force microscope (Park Scientific Instruments M5). A typical RMS roughness of the thermal oxide (SiO_2) layer is about 3 nm.[24]

The equilibrium contact angles between the liquids and the surfaces are measured to evaluate the wetting characteristics using the same method as employed in Schiaffino's experiment.[25] The method basically measures the contact angle of sessile droplets on a solid surface and the data are extrapolated to zero volume to account for the gravitational effect. The contact angles thus obtained are presented in Table II.

A high speed video system (Kodak Ektapro EM, Model 1012) records the spreading and subsequent oscillation of a droplet on a solid surface at a rate of 1000 frames per second. An image stored in the system consists of 192×239 pixels. The illumination is provided by a stroboscope, which is synchronized with the camera, to capture very sharp images. The images stored in the digital memory are downloaded onto a video tape using an S-VHS video tape recorder, and analyzed by an image analysis software, which is capable of measuring the dimensions of objects by the number of pixels. An object of a known size (8 mm in diameter) is recorded by the same video setup and used for calibration. In addition, to obtain highly accurate conditions of the droplet impact, the weight of the droplet is measured for each experiment using a high-precision balance (Mettler Toledo, Model AB104). The diameter deduced by the weight-measurement method is compared with that obtained by the image calibration. The diameters measured by both methods are in very close agreement in all cases, with less than 2% discrepancy. Using the image analysis software, we measure

the base diameter of the droplet at each frame to determine the temporal evolution of droplet shapes.

III. MODELING

As mentioned earlier, we model the spreading and recoiling of a droplet by adopting the variational principle instead of solving the Navier–Stokes equation with moving boundaries. We assume two different droplet shapes in applying the variational method, i.e., a cylinder and a truncated sphere. It is noted that the accuracy of a model critically depends on how closely the assumed shape in the model resembles the real droplet. It is shown in Sec. IV that depending on the impact conditions, one shape assumption results in better prediction than the other for different recoiling behavior. Kendall and Rosehnow[19] were first to use the variational principle assuming the cylindrical shape, in modeling the droplet dynamics. However, they did not consider the interaction of the liquid droplet with a solid surface and the viscous effects. Our model substantially extends their cylinder model to include the wetting properties of the liquid droplet with a solid surface and frictional dissipation. A variational method using a truncated-sphere shape assumption was derived by Bechtel *et al.*[20] In this work, we modify the frictional dissipation term employed in their model.

A. Problem formulation using a cylinder model

We use the variational principle[26] to describe the motion of a droplet colliding with a solid surface:

$$\int_{t_1}^{t_2}(\delta T^* - \delta V^* + \delta W_f^*)dt^* = 0, \tag{1}$$

where T^* denotes the kinetic coenergy of the droplet, i.e., the complementary state function of the kinetic energy,[26] V^* the potential energy, and t^* the time. The frictional work δW_f^* is expressed as

$$\delta W_f^* = -F^*\delta y^*, \tag{2}$$

where F^* denotes the frictional force and y^* the displacement of the frictional motion. In cases where the frictional force is due to the wall shear stress, we write Eq. (1) as

$$\int_{t_1}^{t_2}\left[\delta(T^*-V^*) - \int_{A_b^*}\tau^*\delta\Delta_r^*\,dA^*\right]dt^* = 0, \tag{3}$$

where τ^* is the shear stress at the base of the droplet, Δ_r^* the radial displacement, and A_b^* the base area. Each term in the integrand can be evaluated when the shape of the deforming droplet and the velocity profile are known.

The initial velocity and the diameter of the original droplet before collision are U^* and D^*, respectively. The droplet has the density ρ, the surface tension σ, and the viscosity μ. We choose D^* and $(\sigma/\rho D^*)^{1/2}$ as the characteristic length and velocity scales, respectively. We note that most studies addressing the ''initial spreading'' of droplets employ an inertial spreading time, D^*/U^*, as a characteristic time scale. However, the time scale that best characterizes the recoiling motion driven by capillary action is the characteristic oscillation period of a freely vibrating droplet $(\rho D^{*3}/\sigma)^{1/2}$, and this scale has been adopted in Refs. 17 and 20 for the studies of oscillating droplets on solid surfaces. Moreover, Wachters and Westerling[27] and Foote[28] showed that the time it takes for a colliding droplet to bounce off the contact surface due to vigorous vibration is close to the free oscillation period. Thus we choose $(\rho^* D^{*3}/\sigma)^{1/2}$ as our time scale. The following quantities are nondimensionalized based on those scales unless noted otherwise, and their forms are summarized in Appendix A.

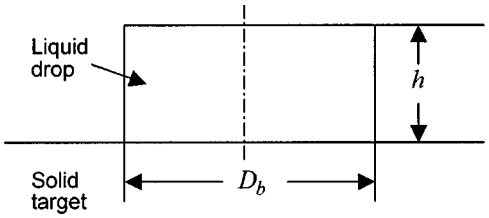

FIG. 2. Geometry of the cylinder model.

The cylinder model assumes the droplet on a solid surface as a cylinder whose nondimensional base diameter and height are D_b and h, respectively, as shown in Fig. 2. The volume of the cylinder is the same as that of the droplet, thus

$$D_b^2 h = \tfrac{2}{3} \tag{4}$$

is satisfied for any t. If either D_b or h is specified in time, the other is known by Eq. (4). Therefore, it is sufficient to simulate the temporal evolution of either D_b or h to fully describe the dynamics of the oscillating cylinder.

The evaluation of the kinetic coenergy is essentially the same as that of Kendall and Rosehnow. Assuming axisymmetric motion and taking the linear velocity-momentum relation (Ref. 26, pp. 19 and 20), the nondimensional kinetic coenergy is written as

$$T = \int_\Omega (v_z^2 + v_r^2)\,d\Omega, \tag{5}$$

where v_z and v_r denote the nondimensional axial and radial velocity of the flow inside the cylinder, respectively, and Ω is the volume. For the energy and volume scales, we choose $\pi\sigma D^{*2}/12$ and $\pi D^{*3}/6$. We relate the axial velocity, v_z, with h as

$$v_z = \frac{z}{h}\dot{h}, \tag{6}$$

where the overdot denotes the time derivative. The radial velocity, v_r, is given by continuity as

$$v_r = -\frac{1}{2}\frac{r}{h}\dot{h}, \tag{7}$$

where r is the nondimensional radius. The flow field given by Eqs. (6) and (7) is that of the potential flow which satisfies the Laplace equation. Substituting Eqs. (6) and (7) into Eq. (5) and performing integration over the volume of the cylinder, we obtain

$$T = \frac{1}{3}\dot{h}^2\left(1 + \frac{1}{16h^3}\right). \tag{8}$$

The potential energy of the system consists of the surface energy and the gravitational energy. The surface potential energy is a sum of the energy of the cylinder surface in contact with gas, $\pi\sigma(D_b^* h^* + D_b^{*2}/4)$, and that of the bottom surface touching the solid surface, $\pi D_b^{*2}(\sigma_{SL} - \sigma_{SG})/4$.[29] Here σ_{SL} and σ_{SG} denote the interfacial tensions or free energy densities, associated with the solid–liquid and solid–gas interfaces, respectively (Ref. 30, p. 58). Assuming that the interfacial energy densities stay constant while a droplet moves on the surface, the difference of σ_{SL} and σ_{SG} can be obtained using Young's equation, i.e., $\sigma\cos\theta = \sigma_{SG} - \sigma_{SL}$, where θ is the equilibrium contact angle between the liquid droplet and the solid surface. Mao *et al.*[31] also suggested that the equilibrium contact angle be used in evaluating the surface energy of the solid–liquid interface.

The gravitational potential energy can be ignored when its change is small as compared to the change of the interfacial energy. The change of the gravitational energy during droplet motion, ΔV_g^*, is scaled as $\Delta V_g^* \sim \rho\Omega^* g R^*$, where R^* is the radius of a droplet. The change of the interfacial energy, ΔV_s^*, can be scaled as $\Delta V_s^* \sim \pi\sigma D^{*2}(D_{\max}^2 - 1)$, where $D_{\max}$ is the ratio of the maximum spread diameter to the original droplet diameter. Thus the relative magnitude of the gravitational energy to the interfacial energy is scaled as $\Delta V_g^*/\Delta V_s^* \sim (1/12)\mathrm{Bo}/(D_{\max}^2 - 1)$, where the Bond number, $\mathrm{Bo} = \rho g D^{*2}/\sigma$. In the experiments whose results are compared with the current modeling later in this paper, the values of $\Delta V_g^*/\Delta V_s^*$ are commonly less than 0.1. Therefore, we neglect the gravitational effect in evaluating the potential energy. The total potential energy of the cylinder is thus, in a dimensionless form,

$$V = 3D_b^2\left[\frac{4h}{D_b} + (1-\cos\theta)\right]. \tag{9}$$

It is noted that our potential energy evaluation is different from that of Kendall and Rosehnow in that ours takes the interfacial energy between the liquid and solid surfaces into account. By using Eq. (4), we express the potential energy as

$$V = 2\left[2(6h)^{1/2} + \frac{(1-\cos\theta)}{h}\right]. \tag{10}$$

The dissipative work is estimated in a similar manner to Bechtel *et al.*[20] Since the potential flow field we obtained above does not afford the viscous effects, we estimate the external viscous stress, τ^*, based on that of an oscillating stagnation flow with the period $(\rho^* D^{*3}/\sigma)^{1/2}$. The stress τ^* is written as

$$\tau^* = \mu\frac{v_r^*}{\delta_H^*}, \tag{11}$$

where μ is the viscosity. The characteristic hydrodynamic boundary layer thickness, δ_H^*, of the oscillating flow, is scaled as[32]

$$\delta_H^* \sim \left(\frac{\mu^2 D^{*3}}{\rho\sigma}\right)^{1/4}. \tag{12}$$

Choosing $(\mu^2\sigma/\rho D^{*3})^{1/2}$ as the stress scale, we obtain the following nondimensional expression for the viscous stress:

$$\tau = F_d\frac{v_r}{\mathrm{Oh}^{1/2}}, \tag{13}$$

where F_d is the dissipation factor, which is determined empirically through comparison between the experimental and modeling results. A detailed discussion on the dissipation factor is given in Appendix B. Oh is the Ohnesorge number defined as

$$\mathrm{Oh} = \frac{\mu}{(\rho D^*\sigma)^{1/2}}. \tag{14}$$

The radial displacement, Δ_r, is written as

$$\Delta_r = \int v_r\, dt. \tag{15}$$

Substituting Eq. (7) into Eq. (15), we obtain

$$\Delta_r = -\tfrac{1}{2} r\ln h, \tag{16}$$

where we arbitrarily set the integration constant to zero since $\delta\Delta_r$ is of our interest here.

Performing the variation of the kinetic coenergy with respect to h and using integration by parts, we get

$$\int_{t_1}^{t_2}\delta T\, dt = -\frac{1}{3}\int_{t_1}^{t_2}\left[2\ddot{h}\left(1+\frac{1}{16h^3}\right) - \frac{3}{16}\frac{\dot{h}^2}{h^4}\right]\delta h\, dt. \tag{17}$$

By a similar procedure, we obtain

$$\delta V = 2\left[\frac{6^{1/2}}{h^{1/2}} - \frac{(1-\cos\theta)}{h^2}\right]\delta h \tag{18}$$

and

$$\delta W_f = \frac{F_d}{24}\mathrm{Oh}^{1/2}\frac{\dot{h}}{h^4}\,\delta h. \tag{19}$$

On substituting Eqs. (17), (18), and (19) into Eq. (3), we require that the coefficient of δh should be zero for the variational formula to be satisfied. In consequence, we finally obtain an equation to describe the temporal evolution of h:

$$\ddot{h} - A(h)\dot{h}^2 + B(h)\dot{h} + C(h) = 0. \tag{20}$$

The coefficients are given by

$$A(h) = \tfrac{3}{32}h^{-1}(h^3 + \tfrac{1}{16})^{-1}, \tag{21}$$

$$B(h) = \tfrac{2}{3}F_d A(h)\mathrm{Oh}^{1/2}, \tag{22}$$

and

$$C(h) = 32A(h)[6^{1/2}h^{7/2} - (1-\cos\theta)h^2]. \tag{23}$$

The initial conditions, i.e., h and $\dot{h}$ at $t=0$, should be specified to solve Eq. (20). Since the original droplet and a cylinder have a substantial difference in shape, we seek initial conditions that will ensure that the initial kinetic coenergy and potential energy of the cylinder are the same as those of the original droplet. In addition, the volume must be conserved as stated in Eq. (4). The equality of initial potential energies of the original droplet and of a cylinder yields the following relation:

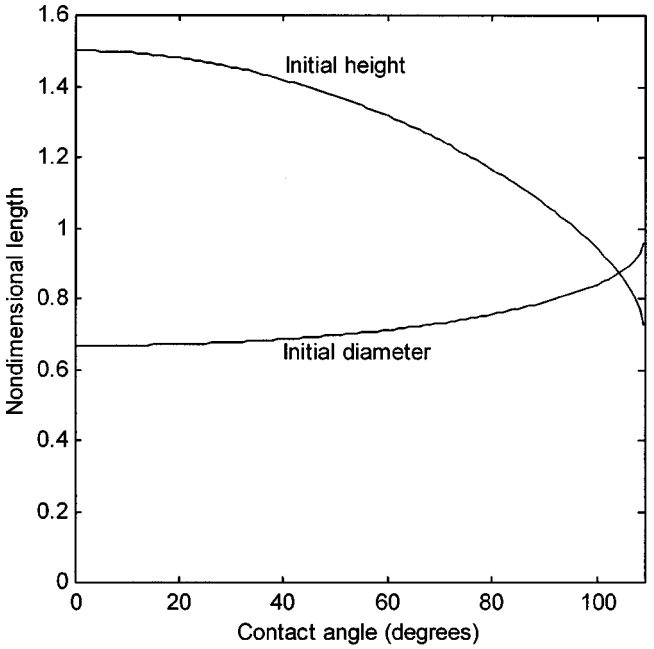

FIG. 3. Initial diameter and height of the cylinder vs contact angle.

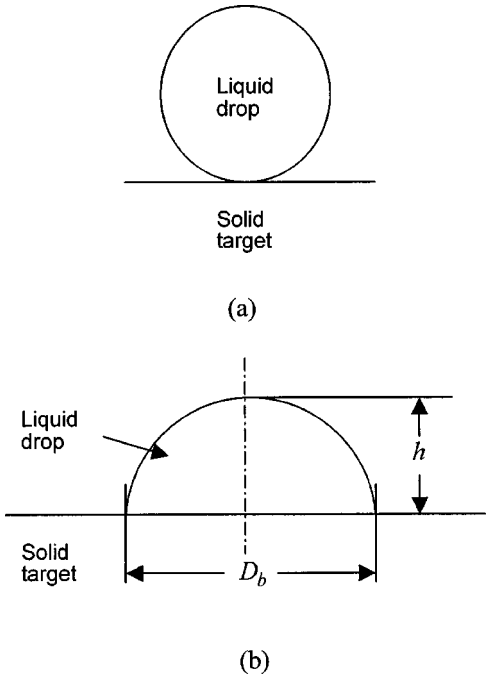

FIG. 4. Geometry of the truncated-sphere model. (a) Initial shape of the sphere at impact. (b) Assumed shape of a droplet during spreading and recoiling.

$$h(0)=\frac{1}{D_b(0)}-\frac{(1-\cos\theta)}{4}D_b(0). \tag{24}$$

Further arrangement of Eq. (24) is made by using Eq. (4):

$$\frac{(1-\cos\theta)}{8}D_b^3(0)-\frac{1}{2}D_b(0)+\frac{1}{3}=0. \tag{25}$$

Therefore, Eq. (25) determines the initial diameter of the cylinder and the initial height is then given by either Eq. (4) or (24). We note that the initial diameter and height of the cylinder depends solely on the contact angle, θ, and Fig. 3 shows initial D_b and h versus θ. The initial $\dot{h}$ is determined by the equality of the kinetic coenergies of the original droplet and of a cylinder:

$$\dot{h}(0)=-\left[3\,\mathrm{We}\left(1+\frac{1}{16h^3(0)}\right)^{-1}\right]^{1/2}, \tag{26}$$

where We is the Weber number defined as $\mathrm{We}=\rho U^{*2}D^*/\sigma$.

Alternatively, the temporal evolution of the base radius, $R=D_b/2$, can be expressed as the following, which is equivalent to Eq. (20):

$$\ddot{R}-\tilde{A}(R)\dot{R}^2+\tilde{B}(R)\dot{R}+\tilde{C}(R)=0. \tag{27}$$

Here the coefficients are given by

$$\tilde{A}(R)=3R^{-1}-\tfrac{1}{3}R^{-3}\Gamma(R), \tag{28}$$

$$\tilde{B}(R)=\tfrac{2}{3}F_d\Gamma(R)\mathrm{Oh}^{1/2}, \tag{29}$$

and

$$\tilde{C}(R)=-96R^3\Gamma(R)[\tfrac{1}{216}R^{-7}-\tfrac{1}{36}(1-\cos\theta)R^{-4}], \tag{30}$$

where

$$\Gamma(R)=\tfrac{9}{16}R^2(\tfrac{1}{216}R^{-6}+\tfrac{1}{16})^{-1}. \tag{31}$$

In summary, the cylinder model presented here is based on the modeling of Kendall and Rosehnow[19] on an inviscid cylindrical drop in the air. We added the effects of wetting between the liquid and the solid, and the frictional dissipation. To evaluate the frictional dissipation, the Bechtel *et al.*[20] dissipation model was employed with modification. Our cylinder model yields the second order nonlinear differential equation, Eq. (20) or (27), which completely describes the dynamics of a liquid cylinder impacting on a solid surface. The initial value problem can be solved numerically with the initial conditions specified by Eqs. (25) and (26), combined with Eq. (4).

B. Problem formulation using a truncated-sphere model

In this section, we present the Bechtel *et al.*[20] truncated-sphere model with the estimation of the frictional term modified. The geometry of a truncated sphere is shown in Fig. 4. Bechtel *et al.* assumed the same velocity profiles as in the cylinder model above. Following the same procedure as the above formulation using a cylinder model, the equation for the temporal evolution of h is given by (for detailed derivation, see Ref. 20)

$$2E(h)\ddot{h}-G(h)\dot{h}^2+I(h)\dot{h}+J(h)=0, \tag{32}$$

where the coefficients are given by

$$E(h)=\left[\frac{M'(h)}{M(h)}\right]^2\left(\frac{13}{180}h^5+\frac{11}{144}h^2+\frac{1}{72}h^{-1}\right), \tag{33}$$

$$M(h)=\tfrac{1}{6}(2h+h^4), \tag{34}$$

$$G(h)=\left(\frac{13h^4}{36}+\frac{11h}{72}+\frac{h^{-2}}{72}\right)\left(\frac{1}{3}+\frac{2h^3}{3}\right)\left(\frac{h}{3}+\frac{h^4}{6}\right)^{-2}+\left(\frac{13h^5}{90}+\frac{11h^2}{70}+\frac{h^{-1}}{36}\right)\left(\frac{1}{3}+\frac{2h^3}{3}\right)\cdot\left[2h^2\left(\frac{h}{3}+\frac{h^4}{6}\right)-\left(\frac{1}{3}+\frac{2h^3}{3}\right)^2\right]\cdot\left(\frac{h}{3}+\frac{h^4}{6}\right)^{-3}, \tag{35}$$

$$I(h)=\psi(h^4-2h+h^{-2})\left(\frac{1}{3}+\frac{2}{3}h^3\right)^2\left(\frac{h}{3}+\frac{h^4}{6}\right)^{-2}, \tag{36}$$

and

$$J(h)=2[4h-h^{-2}+\cos\theta(2h+h^{-2})]. \tag{37}$$

The parameter ψ is given, in the present nondimensionalization, by

$$\psi=\beta\cdot\mathrm{Oh}, \tag{38}$$

where β is related to the boundary layer thickness of an oscillating flow with the period $(\rho^*D^{*3}/\sigma)^{1/2}$. Now we modify the Bechtel *et al*. model to include the dissipation factor, F_d, in the estimation. Thus, β is given by

$$\beta=\frac{F_d}{\mathrm{Oh}^{1/2}}. \tag{39}$$

As mentioned above, the value of F_d is empirically determined as discussed in Appendix B.

The base diameter is related to h by

$$D_b=2[\tfrac{1}{3}(h^{-1}-h^2)]^{1/2}. \tag{40}$$

Since the initial droplet shape assumed by this model exactly represents the real spherical shape, the initial conditions are obtained straightforwardly. The initial height is set equal to the original diameter of the droplet and the initial velocity is set equal to the velocity of the droplet prior to collision. After nondimensionalization, we write

$$h(0)=1 \tag{41}$$

and

$$\dot{h}(0)=-\mathrm{We}^{1/2}. \tag{42}$$

However, we note that while the exact value of the initial kinetic coenergy is $\pi\rho^*D^{*3}U^{*2}/12$, its value given by this model is $13\pi\rho^*D^{*3}U^{*2}/120$, due to the assumed velocity profile. The values of the initial potential energy are equal automatically since the assumed and real shapes are the same.

We note that the angle between the tangential line of the truncated sphere and the solid surface has no physical meaning. As the cylinder model above always has the contact angle of 90°, the contact angle of the truncated sphere is merely an outcome of the intrinsic shape assumption and of such a shape solely determined by Eq. (32). The value of θ appearing in Eq. (37) is the equilibrium contact angle, which is constant, as shown in Table II. Here we emphasize that the contact angle appearing in our model is not used to define the apparent angle between the tangential lines of an assumed droplet shape and a solid surface, but to evaluate the solid–liquid interface energy.

In summary, we introduced the Bechtel *et al.*[20] model which assumes the droplet as a truncated sphere. However, the evaluation of the frictional dissipation was modified in this work to include the dissipation factor that is to be determined empirically. The second order nonlinear differential equation, Eq. (32), describes the dynamics of a liquid truncated sphere on a solid surface. The initial value problem can be solved numerically with the initial conditions specified by Eqs. (41) and (42).

IV. RESULTS AND DISCUSSION

A. Water droplets

Figure 5 shows the dynamics of water droplets colliding with polycarbonate surfaces. The water droplets, which possess relatively low viscosity and high surface tension as compared with ink and silicone oil droplets, go through vigorous oscillation due to high We and low Oh.[17] Nevertheless, the two droplets in the figure show distinctive impact behavior depending on impact conditions as explained below. The temporal evolution of the oscillating droplet shapes is presented quantitatively in Fig. 6, showing the base diameter vs time until the droplets nearly come to rest. In the figure, the vigorous primary oscillation of a droplet with higher impact inertia is well observed as compared to one with lower inertia. The droplet, which impacts on the surface with higher speed, and thus with greater inertia and higher Weber number, spreads further in the initial spreading process. Figure 6 also shows that, in the subsequent recoiling stages, the droplet with greater inertia retracts more vigorously than one with smaller inertia, and consequently exhibits a smaller base diameter and a higher centerline elevation just prior to respreading [e.g., in Fig. 5, 25.6 ms for (a) and 36.2 ms for (b)]. In Fig. 5 we name the first extension and retraction of the base diameter of a droplet upon impact, the primary spreading, and the primary recoiling, respectively.

The droplets with greater impact inertia show relatively higher motility than those with weaker inertia in the oscillation stages subsequent to the primary recoiling. These subsequent oscillations were experimentally observed by Cheng[13] and Zhang and Basaran.[33] However, motion in those stages is relatively weak compared with the primary motions (see Fig. 6). Therefore, our interest in this work mainly consists in the primary spreading and primary recoiling stages.

Next, we compare the experimental data, especially those of the primary recoiling stage, with the predictions of the models, in Fig. 7. The results of both the cylinder model and the truncated-sphere model are presented. In the low-impact inertia case as shown in Fig. 7(a), both the cylinder model and the truncated-sphere model show qualitatively good agreement with the experimental data. It is noted that the cylinder model overestimates the strength of recoiling, while the truncated-sphere model underestimates it. In Fig. 7(b), where impact inertia is higher than that in Fig. 7(a), the cylinder model closely predicts the experimental data. On the other hand, the truncated-sphere model deviates significantly

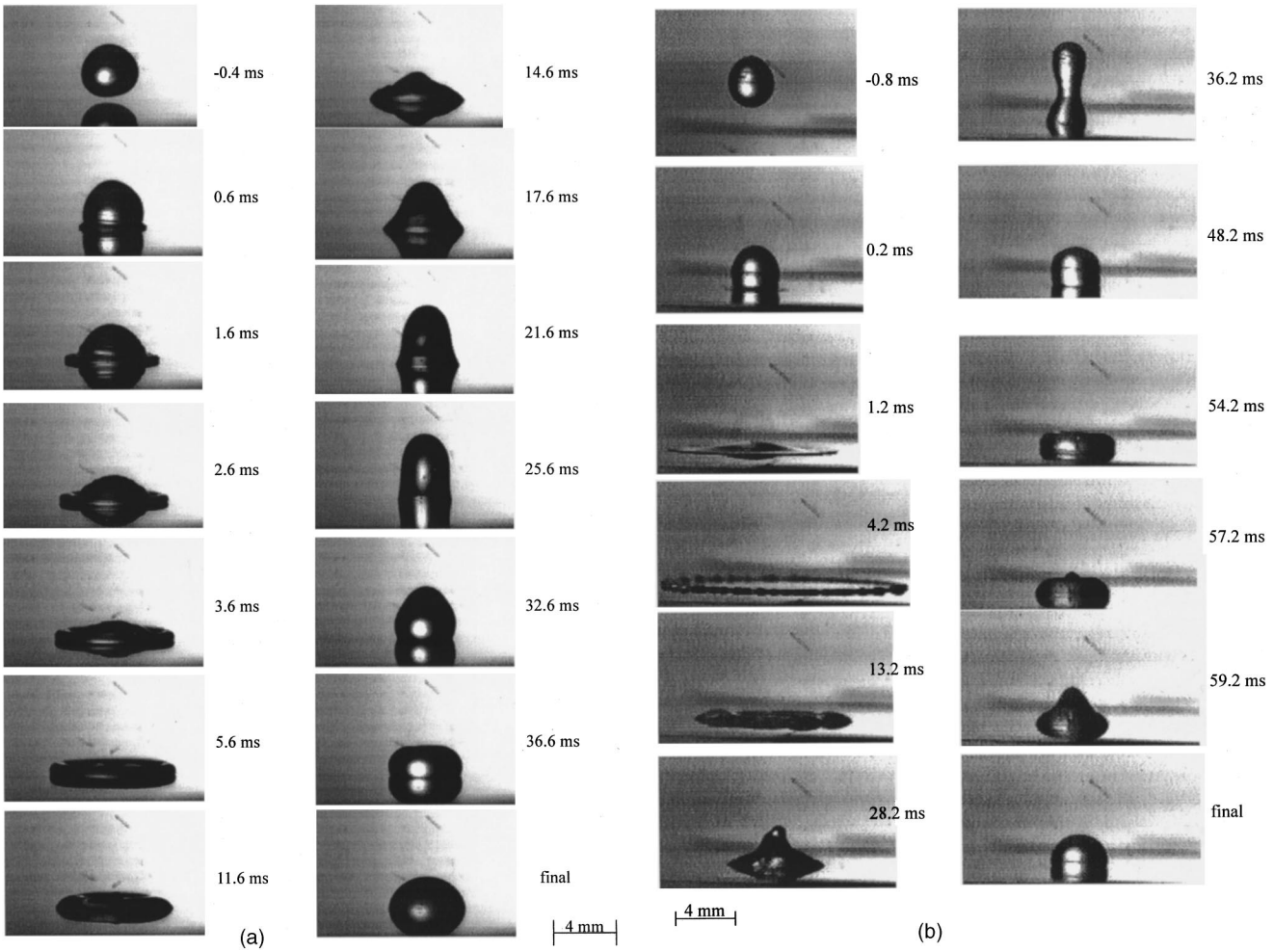

FIG. 5. Images of a water droplet colliding with a polycarbonate surface. (a) Original droplet diameter=3.6 mm, Impact velocity=0.77 m/s, We=30 and Oh=0.0017. (b) Original droplet diameter=3.5 mm, impact velocity=3.47 m/s, We=582, and Oh=0.0017.

from the experimental data, failing to predict the strong recoiling. Figure 7(c), where the impact inertia is even higher, shows the closer agreement between the cylinder model and the experimental results, while the truncated-sphere model deviates even more.

We note that the truncated-sphere model results are close to the experimental data when t is large ($t=2$). This is because the steady-state shape of the truncated-sphere model and the actual sessile droplet are identical. Here the steady state implies when the time derivatives in Eq. (32) vanish, thus the steady-state shape is given by $J(h)=0$. Since the radii of the droplets used in these experiments (1.6 to 1.8 mm) are less than the capillary length of water, $\kappa^{-1}=(\sigma/\rho g)^{1/2}=2.7$ mm, the deformation of the sessile drops from a truncated-sphere shape due to gravity, is small.[34]

Figure 8 shows the droplet dynamics longer than Fig. 7 to better illustrate this statement. While the droplets, whose behavior is illustrated in Fig. 7, generally show weak base-diameter oscillations after $t=2$, the droplet in Fig. 8 retains its motility longer than those droplets owing to its higher impact inertia (see also Fig. 6). Again, the cylinder model predicts the primary recoiling fairly accurately, and the truncated-sphere model's prediction approaches the equilibrium state slowly as exhibiting a great discrepancy from experimental results. It is emphasized that in all the simulations shown in Figs. 7 and 8, a single value of dissipation factor has been used for each model (Table III).

When the impact inertia is high, i.e., We is high, fingers develop at the rim of a spreading droplet due to the Rayleigh–Taylor instability of the decelerating spreading front.[11,18,35] The image at 4.2 ms of Fig. 5(b) shows the typical fingers. However, the fingering is supposed to have insignificant effects on measurement and prediction of the base diameter considering that the magnitude of the frontal undulations is less than 2% of a local spreading radius even when We reaches 1020 (see Ref. 10) which is much higher than the maximum We used in this study.

So far we have observed that the cylinder model more accurately predicts the experiments than the truncated-sphere model in the primary recoiling stages. This is mainly because the truncated-sphere model predicts slower recoiling than the experiments. This may be explained by investigating the images in Fig. 5, which show that the recoiling water droplet resembles a cylinder more closely than a truncated sphere. The similarity of the droplet shape to a cylinder and its discrepancy from a truncated sphere are more pronounced as the impact inertia increases and thus as the recoiling gets stronger. This is consistent with the observed improvement

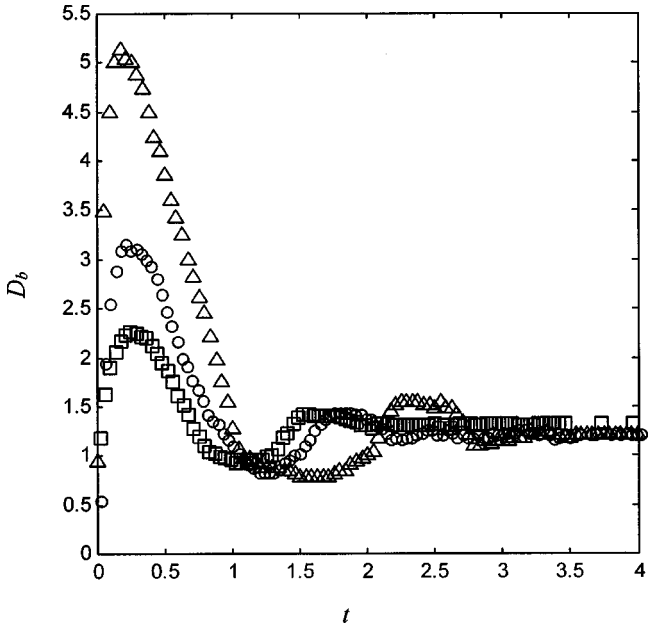

FIG. 6. The temporal evolution of the base diameter of water droplets colliding with a polycarbonate surface. The impact conditions for squares and triangles are the same as those in Figs. 5(a) and 5(b), respectively. The impact conditions for circles: Original droplet diameter=3.7 mm, impact velocity=1.63 m/s, We=137, and Oh=0.0017.

of agreements between the experiments and the cylinder model as inertia increases. This explains the phenomena observed in Fig. 7(a), where the recoiling droplet assumes a shape lying between a cylinder and a truncated sphere. In both Figs. 7 and 8, the cylinder model does not yield an accurate prediction after the primary recoiling stages, since the droplets no longer resemble a cylinder beyond that point. In addition, we note that the truncated-sphere model succeeds in predicting the primary spreading stage fairly accurately. This appears to be because a truncated sphere represents the shape of the collapsing droplet in the primary spreading stages with sufficient accuracy.

To further examine the validity of our model, we compare our modeling predictions with previously reported, experimental and numerically simulated results. In Fig. 9, we compare our predictions with the experimental and numerical results of Fukai *et al.*[14] on water droplets colliding with Pyrex glass and wax coated plates. Their numerical simulation solved the full Navier–Stokes equation, as mentioned in the Introduction. In this paper, we used a cylinder model since Oh and We of these experiments fall into a regime where a cylinder model is expected to be more accurate (see above and also Sec. IV E). The figure shows that the agreement of our modeling with their experimental results are generally good. Moreover, comparing the computational efforts to solve the full Navier–Stokes equation and to solve a single differential equation such as Eq. (27), the efficiency of our model becomes apparent.

B. Ink and silicone oil droplets

Ink and silicone oil, the liquids whose behavior will be discussed in this section, possess physical properties that differ significantly from those of water. For example, they have a greater viscosity and a smaller surface tension than water. It is shown here that these differences make substantial changes in the droplet impact behavior. Figure 10(a) shows images of an ink droplet colliding with a polycarbonate surface. Although the ink droplet has comparable size, equilibrium contact angle, and impact speed to those of the water

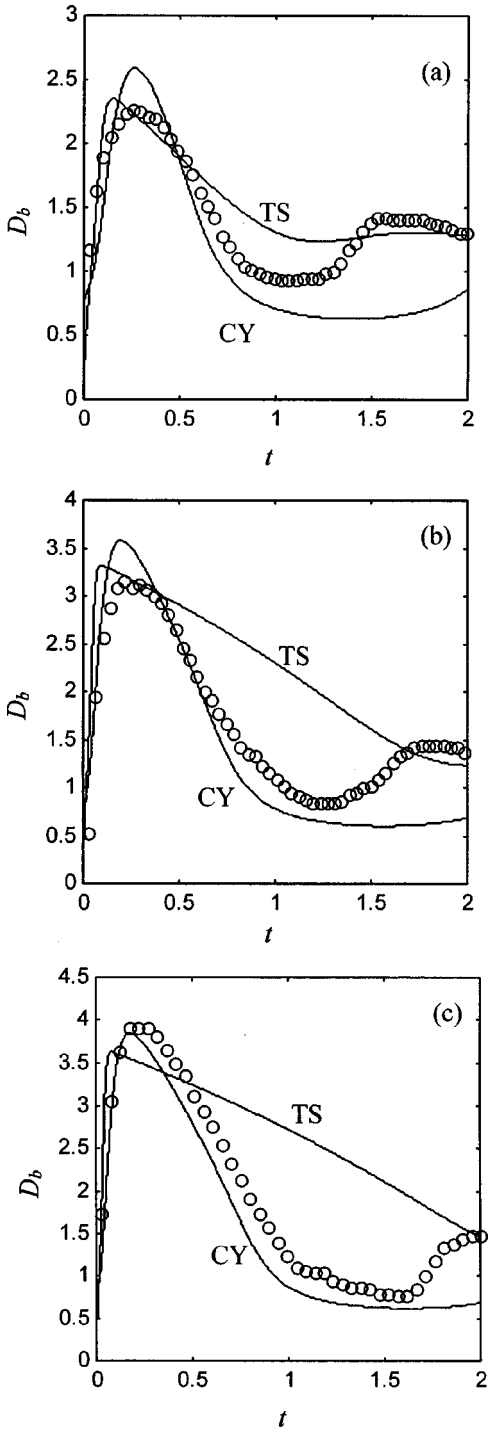

FIG. 7. Predictions of the models and the experimental measurements for water droplets on a polycarbonate surface. Modeling results using the cylinder model (CY) and the truncated-sphere model (TS) are both presented. Beyond the time range shown here, the base diameter change is negligibly small. (a) We=30 and Oh=0.0017, (b) We=137 and Oh=0.0017, (c) We =207 and Oh=0.0018.

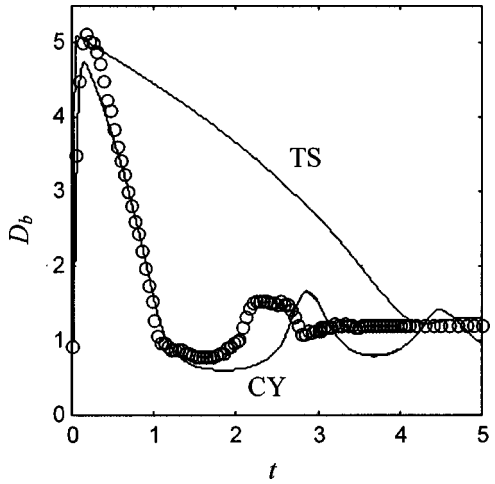

FIG. 8. Behavior of a water droplet on a polycarbonate surface until $t=5$. CY and TS denote the cylinder model and the truncated-sphere model, respectively. We=582 and Oh=0.0017.

droplet in Fig. 5(b), their behaviors, especially their recoiling motions, are very different. The ink droplet does not recoil as vigorously as the water droplet but rather, recoils gradually until it reaches its equilibrium shape. Due to this weak primary recoiling, the subsequent re-spreading and oscillation are absent in this case. At this point, we may qualitatively remark that the high viscosity of the ink induces a large resistance to a recoiling flow and also that the restoring force is weak due to a small surface tension. These combined factors contribute to the relatively weak recoiling motion. More discussion on this is postponed to the following sections. The motion of a silicone oil droplet impacting with a polycarbonate surface is shown in Fig. 10(b). Silicone oil has a viscosity two orders higher than that of water and it also has a very low equilibrium contact angle on polycarbonate. Due to its high viscosity, its droplet spreads less than those of the other liquids in the primary spreading stage, and it shows only slight recoiling. Afterwards, since the droplet wets the surface almost perfectly in its equilibrium state, the droplet respreads slowly until it comes to rest as a thin film.

After examining both Figs. 10(a) and 10(b), which show the shapes of the recoiling droplets, a truncated-sphere model seems a clear choice to predict the dynamics of ink and silicone oil droplets. Figure 11 shows the experimental results and model predictions. The predictions of the truncated-sphere model agree with the experimental results surprisingly well, considering the approximate nature of the model. The figure shows the base diameter of an ink droplet impacting on a silicone oxide surface as well as on a polycarbonate surface. The effect of the target surface on the recoiling process will be discussed in Sec. IV D.

TABLE III. Dissipation factors used in this work.

Liquid	Assumed shape in model	F_d
Water	Cylinder	15
Water	Truncated sphere	5.3
Ink	Truncated sphere	3.2
Silicone oil	Truncated sphere	3.2

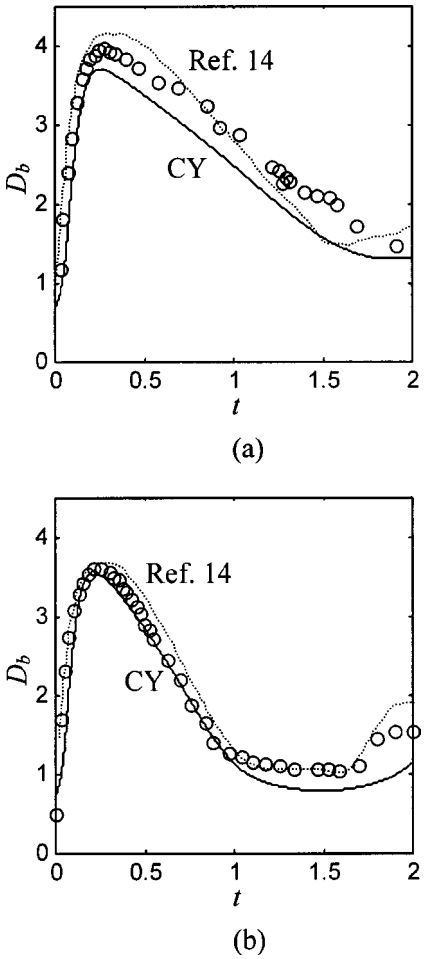

FIG. 9. Comparison of Fukai *et al.* (Ref. 14) results and the predictions by a cylinder model. Circles denote experimental results by Fukai *et al.* In the figure, Ref. 14 and CY denote the computation results of Ref. 14 and of our cylinder model, respectively. In the cylinder model, the same dissipation factor as droplets on polycarbonate, i.e., $F_d=15$, was used. (a) Water droplet on a Pyrex glass plate. We=115, Oh=0.001 68, and $\theta=54°$. (b) Water droplet on a wax coated plate. We=128.2, Oh=0.001 68, and $\theta=76°$.

C. Effects of Weber and Ohnesorge numbers

So far we have presented the experimental results obtained by varying such conditions as droplet liquids, target surfaces, and impact inertia. It has also been shown that the approximate models predict the experimental measurements fairly well. The models we employ state that the motion of the droplet, more specifically the temporal evolution of a nondimensional base diameter, is governed by the Weber number, the Ohnesorge number, and the equilibrium contact angle. This is consistent with Schiaffino and Sonin's[17] result of a similarity analysis for the liquid deposition process.

The Weber number, a measure of the impact inertia compared to the surface energy, appears only in the initial conditions, while the Ohnesorge number and the contact angle exclusively appear in the equations governing the droplet dynamics. Consequently, both of the models roughly state that We determines the initial spreading stage and that

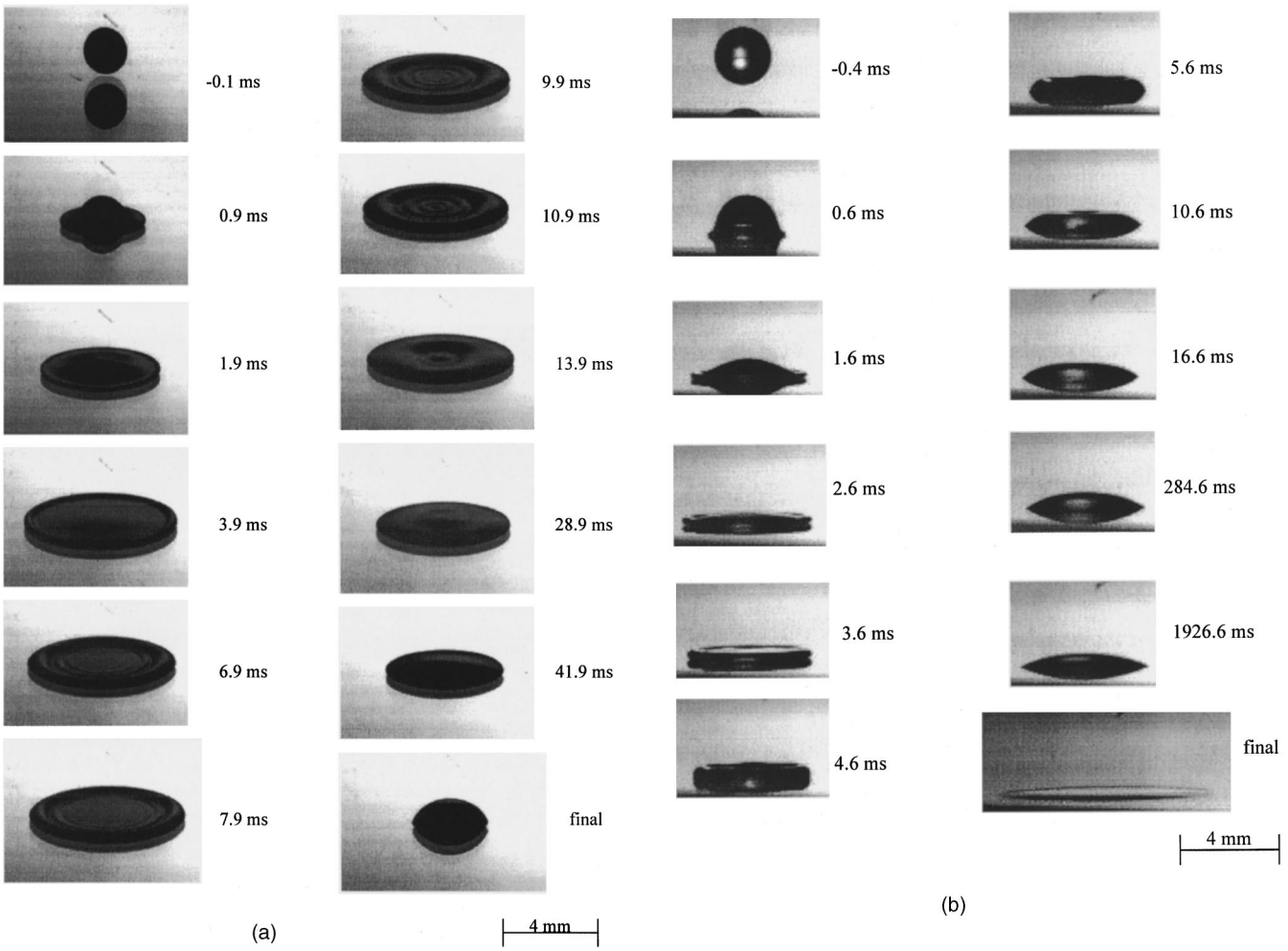

FIG. 10. (a) Images of an ink droplet colliding with a polycarbonate surface. Original droplet diameter=3.2 mm, impact velocity=1.75 m/s, We=190, and Oh=0.0060. (b) Images of a silicone oil droplet colliding with a polycarbonate surface. Original droplet diameter=2.8 mm, impact velocity=1.44 m/s, We=166, and Oh=0.109.

the following droplet motion is, under the influence of the previous motion history, ruled by Oh and θ. The foregoing statement is consistent with the observation of Schiaffino and Sonin[17] that the early stage of spreading is mainly governed by the inertial effect (We) and that the later stage, where droplet motion is slow, is appropriately described by Oh and θ. This section discusses the role of We and Oh and the next section will address the effect of the contact angle.

The Ohnesorge number scales the resisting force in the recoiling process. As shown above, whether an impacting droplet will assume a shape close to a cylinder or a truncated sphere depends on the strength of recoiling. An ink droplet has a relatively high viscosity and a low surface tension, thus a high Oh, which implies that the resistance is dominantly due to viscosity. Therefore, the flow induced by the capillarity force is entirely dissipated by the viscosity and the recoiling is relatively slow. As a result, the recoiling droplet does not deviate much from the truncated sphere. On the other hand, a water droplet has a relatively low viscosity and a high surface tension, thus low Oh. This implies that the resistance is caused by the inertia as well as the viscosity. Therefore, the potential energy stored in an excessively spread state is partially converted into kinetic energy associated with the recoiling motion, despite the viscous dissipation. Hence, the water droplets recoil faster and a cylinder is the more appropriate shape to model the vigorously recoiling droplet.

The foregoing argument is verified by Fig. 12. The figure shows the relative magnitudes of resisting force terms for recoiling (inertia and viscosity) with respect to the driving force term (potential energy) for both the water and ink droplets. For water droplets, the kinetic (inertia) and viscous terms are comparable in the recoiling stage, and both play important roles to balance with the potential term. For ink droplets, however, the kinetic term is negligible, and thus only the viscous term is balanced with the potential term.

From the fact that inertia terms become negligibly small in the ink droplet, it follows that the recoiling motion can be estimated using only viscous and potential terms. Therefore, Eq. (32) reduces to

$$F(h)\dot{h}+G(h)=0, \tag{43}$$

which is the first order equation, thus requiring only one initial condition for h. The initial condition should be satisfied at the time when the recoiling starts, that is, when the

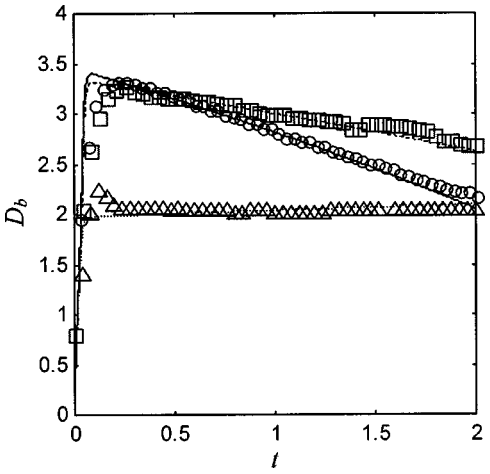

FIG. 11. Spreading and recoiling of an ink droplet (circles, We=190 and Oh=0.0060) and a silicone oil droplet (triangles, We=166 and Oh=0.109) on polycarbonate and an ink droplet on silicon oxide (squares, We=170 and Oh=0.0061). The lines are the modeling results and they agree well with each experimental result.

base diameter (height) reaches its maximum (minimum). It is possible to further simplify Eq. (43) in the limit $h \ll 1$, i.e., when the droplet is very flat, which is usually the case in the beginning of primary recoiling. Then we obtain the following equation:

$$\dot{h} - kh^2 = 0, \tag{44}$$

where $k = 2(1-\cos\theta)/\psi$, k being always positive unless $\theta = 0$. With the initial condition, $h = h_{\min}$, where $h_{\min}$ signifying the minimum height, at $t = t_i$, the solution of Eq. (44) is given by

$$h = \left[\frac{1}{h_{\min}} - k(t - t_i) \right]^{-1}. \tag{45}$$

Expressing Eq. (45) in terms of D_b using Eq. (40) in the limit $h \ll 1$, we obtain a closed form solution for D_b:

$$D_b = [D_{\max}^2 - \tfrac{4}{3}k(t - t_i)]^{1/2}, \tag{46}$$

where $D_{\max}$ is the maximum base diameter at $t = t_i$. Figure 13(a) compares the experimental data during recoiling of an ink droplet with modeling results using the original truncated-sphere model, Eq. (32), and the simplified relations, Eqs. (43) and (46). It is as expected that Eqs. (32) and (43) result in almost identical predictions since inertia terms are negligibly small. However, it is remarkable that the further simplified relation, Eq. (46), generates a fairly close result to that of the original model, notwithstanding the increase of discrepancy as D_b gets smaller, that is, as the limit $h \ll 1$ deviates from the real shape.

Different results are obtained for water droplets when the inertia terms are neglected in the modeling (it is recalled that the inertia terms are not negligible in reality). Using the cylinder model in terms of R, we get the following equation with the inertia terms ignored:

$$\tilde{B}(R)\dot{R} + \tilde{C}(R) = 0. \tag{47}$$

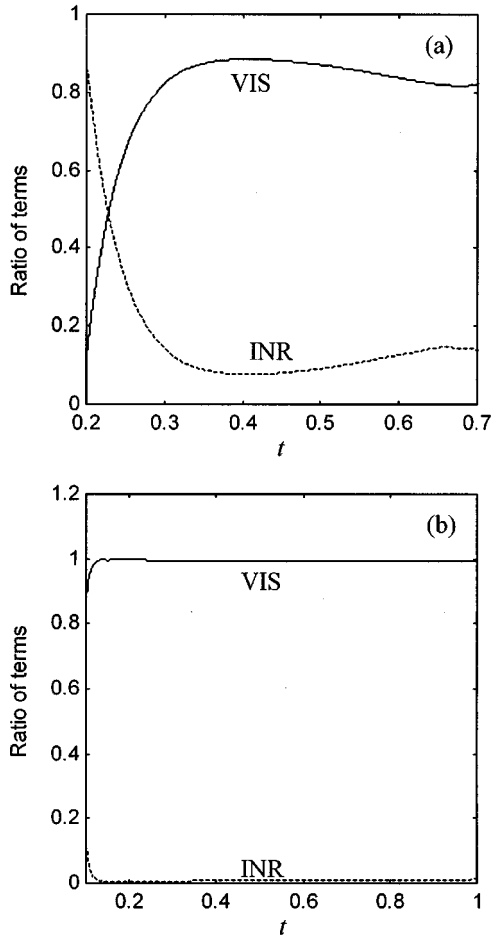

FIG. 12. Relative magnitudes of resisting force term with respect to the driving force term. VIS (INR) denotes the relative magnitude of the viscosity (inertia) term to the potential term. (a) Water droplet on polycarbonate. VIS $= |\tilde{B}(R)\dot{R}|/|\tilde{C}(R)|$ and INR $= |\ddot{R} - \tilde{A}(R)\dot{R}^2|/|\tilde{C}(R)|$ [see Eq. (27)]. We =137 and Oh=0.0017. (b) Ink droplet on polycarbonate. VIS $= |I(h)\dot{h}|/|J(h)|$ and INR $= |2E(h)\ddot{h} - G(h)\dot{h}^2|/|J(h)|$ [see Eq. (32)]. We =190 and Oh=0.0060.

This equation is of the first order and we again need only one initial condition, namely $R = R_{\max}$ at $t = t_i$. Figure 13(b) compares the solutions of Eq. (47) with those of the original model and the experimental results. As predicted, they show considerable difference, indicating the significant effects of kinetic terms even in the recoiling stage.

The recoiling speeds of water droplets, whose diameters range from 3 to 3.7 mm, impacting on the same target surface (polycarbonate) with different velocities are collected in Fig. 14. Although Oh does not change very much (0.001 68 to 0.001 87), varying the Weber number causes a significant difference in the recoiling speed. This is because We determines the maximum base diameter in the primary spreading stage, which becomes the initial condition for the following recoiling motion. Highly spread droplets tend to recoil more vigorously, or faster, owing to the great driving force arising from the large difference between its equilibrium state and the initial (maximum) spread area.

Figure 15 simulates droplet base diameter using the cylinder model to evaluate the individual effects of We and Oh. Figure 15(a) shows that the Weber number plays a critical

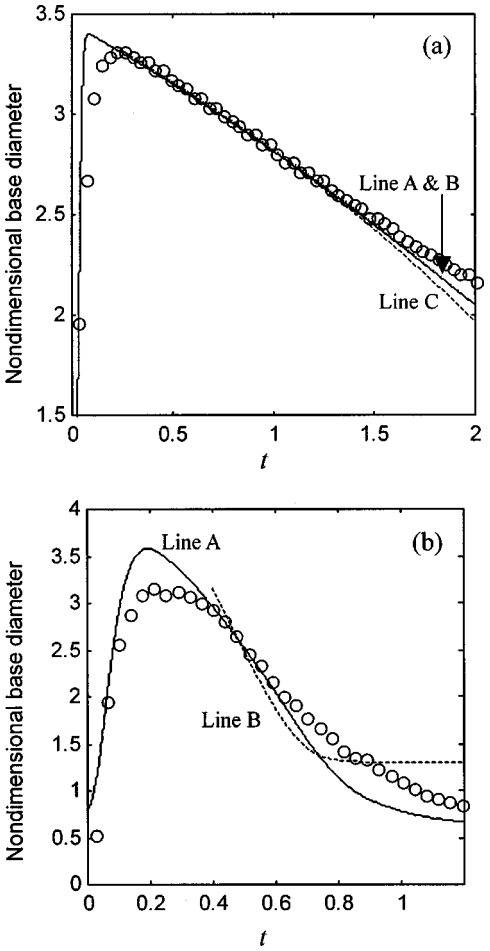

FIG. 13. Simplified modeling results for recoiling. (a) Ink droplet on polycarbonate. We=190 and Oh=0.0060. Lines *A* and *B* are obtained by the original model, Eqs. (32) and (43), respectively, and they are practically undistinguishable. Line *C* is from Eq. (46). Lines *B* and *C* both start from where the experimental base diameter is the maximum ($D_b=3.312$ at $t=0.26$). (b) Water droplet on polycarbonate. We=137 and Oh=0.0017. Line *A* is from the original model and line *B* is from Eq. (47). Line *B* has been shifted to the right by $\Delta t=0.2$ to be better compared with line *A*.

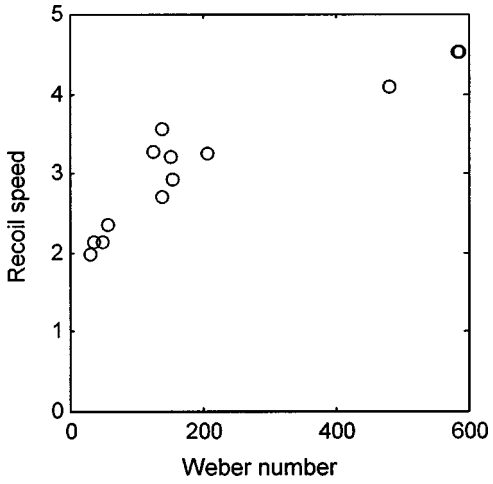

FIG. 14. Nondimensional recoil speed. The Ohnesorge number ranges from 0.0017 to 0.0019. The recoil speed is the average nondimensional velocity of the base diameter from its maximum until it passes the equilibrium diameter during the primary recoiling.

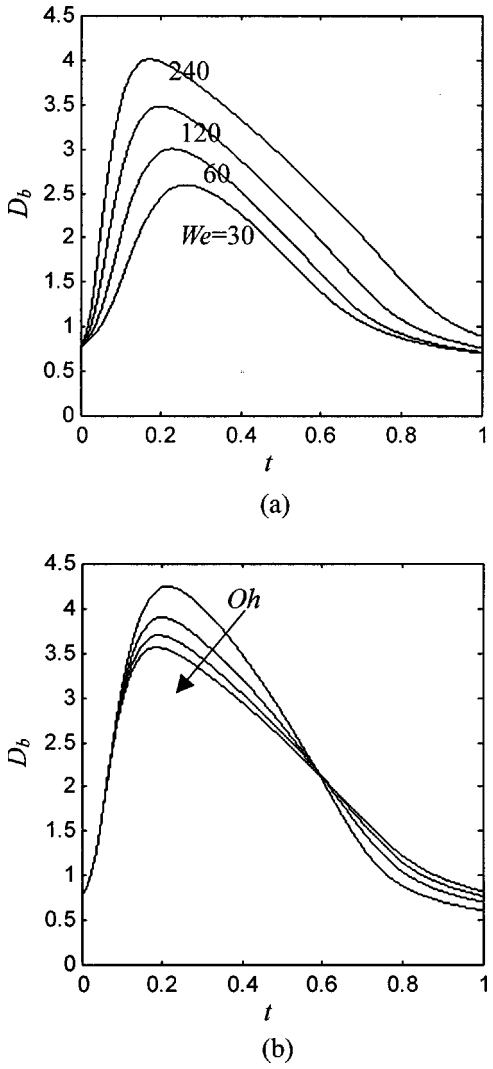

FIG. 15. Individual effect of We and Oh. (a) Oh is fixed at 0.0017 and We varies. (b) We is fixed at 150 and Oh varies. Along the arrow, Oh=0.0005, 0.001, 0.0015, and 0.002.

role in determining the initial spreading process, while the recoiling speed (the downslope in the recoiling stage) is not much affected owing to the constant Oh. On the other hand, when the Weber number is kept constant [Fig. 15(b)], the initial spreading processes are almost identical. However, the recoiling is fairly dependent on the Ohnesorge number in such a way that the droplet with smaller Oh recoils faster. These tendencies are consistent with our experimental observations as discussed above.

D. Effects of the contact angle

This section examines the effects of target solids on the recoiling of water and ink droplets. Our study investigates the dependence of the droplet motion upon target surface materials through measuring the equilibrium contact angles. This is based on the assumption that the recoiling takes place mainly because the base area of the droplet spreads more than its equilibrium state, which is determined by the equilibrium contact angle. Therefore, the equilibrium contact angle, θ, determines the strength of recoiling, and thus we

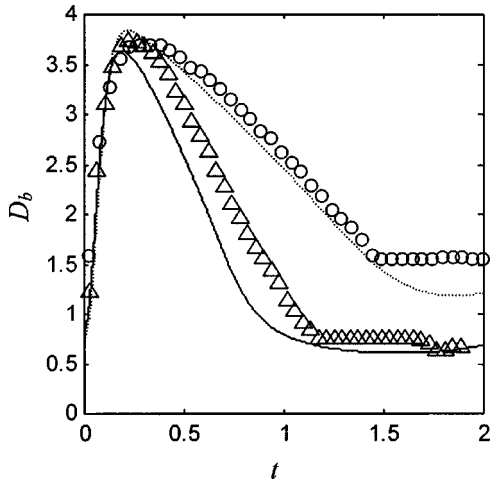

FIG. 16. Effect of wetting on recoiling behavior. The triangles and the solid line represent water droplet on polycarbonate (We=150 and Oh=0.0017). The circles and the dotted line represent water droplet on silicon oxide (We=166 and Oh=0.0019).

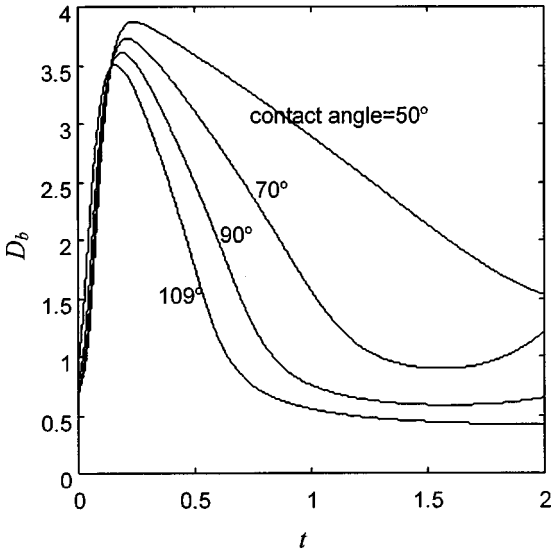

FIG. 17. Effect of the contact angle on the droplet dynamics. The simulations are based on the cylinder model. We=150, Oh=0.0017, and $F_d=15$.

assume that θ is the major parameter to describe the effects of wetting. The models presented in this paper are consistent with this argument as the surface potential energy is evaluated using θ, as shown in Eq. (9), for example. In addition, Ref. 17 suggested that considering the equilibrium contact angle be sufficient to define the phenomena at the contact line at least to the lowest order.

Figure 16 compares the base diameters of water droplets on different target surfaces, polycarbonate and silicon oxide. It is noted that water wets the silicon oxide surface better than the polycarbonate surface (see Table II). Under similar impact conditions, the base diameters in the initial spreading stage are essentially alike since the flow is inertia dominated.[14] However, in the recoiling stage, the droplet impacting on the polycarbonate (poor wetting surface) recoils faster than the droplet on the silicon oxide (good wetting surface). This shows the strong dependence of recoiling upon the wetting between liquid and solid. As the wetting improves, i.e., as the equilibrium contact angle decreases, the recoiling gets slower. We present the predictions of the cylinder model together with the experimental results. The model employing different ''equilibrium'' contact angles for different target surfaces closely predicts the dependence of the recoiling behavior on the wetting. The same behavior is observed in the ink droplet (Fig. 11). As with the water droplet, the ink droplet recoils faster on the poor wetting (polycarbonate) surface than on the good wetting (silicon oxide) surface. The truncated-sphere model employing different ''equilibrium'' contact angles predicts the experimental results surprisingly well for both the target surfaces.

The mechanism of a droplet recoiling faster on a poor wetting solid surface than on a good wetting surface can be easily understood as the following. In equilibrium, a droplet on a poor wetting surface does not spread as much as on a good wetting surface, that is, the poor wetting surface has a weaker affinity for the liquid than the good wetting surface.[30] Therefore, when the droplet spreads wider than its equilibrium state due to its initial impact inertia, the liquid on the poor wetting surface has a stronger tendency to reduce its contact area than one on the good wetting surface. As mentioned above, the models reflect this effect by incorporating the contact angle in the surface energy term. In the cylinder model, as θ increases, the magnitude of $\tilde{C}(R)$ increases [it should be noted that $\tilde{C}(R)$ is positive so as to be balanced, roughly, with the negative $\tilde{B}(R)\dot{R}$ in the recoiling stage where $\dot{R}<0$]. The same applies to the truncated-sphere model where the magnitude of $I(h)$ increases as θ increases—in this case, $I(h)$ is negative since $\dot{h}>0$ in the recoiling stage. Since the potential term corresponds to the driving force of the recoiling motion, higher θ induces faster recoiling. Figure 17 illustrates this effect of θ on the recoiling behavior using the cylinder model.

E. Discussion of the regime for each model

Now we discuss in which conditions the cylinder or the truncated-sphere model would be appropriate. We have shown above that this is equivalent to searching for regimes where the recoiling is resisted entirely by viscosity (truncated-sphere model) and where inertia plays a significant role (cylinder model) in resisting the motion as well as viscosity. In our study, the primary spreading of both the water and ink droplets belongs to the inviscid, impact-driven flow regime[17] since $We \gg 1$ and $Oh \ll We^{1/2}$. However, from the final stages of primary spreading, the viscous effects become significant and the motion gets slow. Consequently, the regime that characterizes the recoiling alters to that of the capillarity-driven flow. In this regime, it is Oh that determines whether the resistance is dominantly viscosity (high Oh) or inertia (low Oh). Therefore, Oh is considered to be the most important parameter to determine which model would be appropriate.

Schiaffino and Sonin[17] suggested that when a droplet ''spreads'' in a capillarity-driven flow regime ($We \ll 1$), the transition from the region where the resistance is primarily

due to inertia, to the region where the resistance is due to viscosity, occur in the broad range of $0.007<\mathrm{Oh}<0.7$, in the present definition of Oh. However, in the ''recoiling'' process studied here, the ink droplets, whose Ohnesorge numbers are approximately 0.006, exhibit highly viscous, capillarity-driven dynamics. On the other hand, the water droplets, whose Ohnesorge numbers are less than 0.002, exhibit such dynamics that the flow is resisted by both inertia and viscosity. Therefore, our experimental results suggest that in the capillarity-driven recoiling flow, $\mathrm{Oh}=0.006$ ($\mathrm{We}<200$, see below for the discussion on We) falls into an entirely viscosity resisted regime. The transition from an inertia resisted regime to a viscosity resisted regime certainly occurs below $\mathrm{Oh}=0.002$. It is important to realize that the cylinder model represents a regime where both inertia and viscosity have significant effects in resisting the flow, and thus this regime corresponds to the aforementioned transition region. It is not possible here to precisely predict the range of the transition region, but our study shows that the range of Oh, corresponding to the transition region for the recoiling flow, is located much lower than that for the spreading motion.

It is worth noting that We also affects the recoiling flow although its effects are minor compared to those of Oh. We have shown that We determines the maximum spread diameter that is the initial condition of the recoiling motion. In addition, its effects on the recoiling speed have been shown in Fig. 14. The lower We gets, the more significant the resistance due to viscosity becomes. Nonetheless, as mentioned above, the effects of We in determining the recoiling flow regime are much weaker than Oh. Especially, when Oh ranges where the corresponding regime completely falls into either the inertia-resisted region or the viscosity-resisted one, We plays a negligible role in determining the flow regime. For example, when We of an ink droplet was increased to approximately 600 while keeping Oh at a constant, the recoiling pattern was the same as that of the low We ink droplets shown here. However, the quantitative analysis of its motion is not presented since at that high We, the ink droplet splattered upon collision with tiny droplets around the periphery splashing off the main body that continued to recoil. This suggests that when Oh is high enough (0.006), the flow remain in the viscosity-resisted regime in spite of an increase of We. As a droplet with a sufficiently low Oh, a mercury droplet can be considered. The experiments of Ref. 17 showed that in the very low We range ($\mathrm{We}\approx 2$), the small mercury droplets with $\mathrm{Oh}\approx 0.0007$ still vigorously recoil upon impact, even disengaging from the surface. Therefore, when Oh is low enough, the recoiling flow belongs to the inertia-resisted regime even when We is very low.

On the other hand, the water droplets with $0.0016<\mathrm{Oh}<0.0019$ considered in this study exhibit the recoiling dynamics belonging to the transition region. In this region, it appears that We plays a relatively important role in determining the flow characteristics. As discussed above, at high Weber numbers, the droplets resemble a cylinder, while at low Weber numbers the shape of droplets tends to approach a truncated sphere (Fig. 5).

It is also noted that θ affects the flow characteristics since it is related to the driving force of the recoiling flow. Especially, in cases where θ is an extreme value, either very close to 0 or 180°, it may alter the flow characteristics. However, when the value of θ lies in a moderate range ($0\ll\theta\ll 180°$), its effects are not so critical as to determine the flow regime.

In summary, our ''experimental'' results suggest that when Oh is higher than 0.006, the truncated-sphere model should be appropriate in modeling the droplet recoiling. In the range of $0.0016<\mathrm{Oh}<0.0019$, the cylinder model closely estimates the recoiling when We is high ($\mathrm{We}>30$). As Oh decreases to even lower values, the cylinder model is expected to predict the droplet dynamics more accurately with less dependence on We. The determination of the exact transition region calls for more study, but our discussion suggests that Oh play a major role in characterizing the flow, while We has relatively minor effects.

V. CONCLUDING REMARKS

In this paper, we have investigated the recoiling behavior of water, ink, and silicone oil droplets upon collision with different solid surfaces. In the experiments, images of the impacting droplets were captured sequentially by a high speed video system. The images were analyzed to obtain the temporal evolution of the base diameter of the droplet. To understand the physics underlying the recoiling, we developed a model based on the variational principle, assuming the droplet shape to be cylindrical, and modified the truncated-sphere model of Bechtel *et al.* to accommodate the dissipation factor. The models and the experimental results were in good agreement for various dynamic and wetting conditions. It was shown that when Oh is low ($\mathrm{Oh}<0.002$, say), the cylinder model appropriately predicts the droplet recoiling dynamics and that when Oh is high ($\mathrm{Oh}=0.006$), the truncated-sphere model is appropriate.

Using these models, a significant computational effort is saved by solving a single second-order, nonlinear differential equation instead of solving the full Navier–Stokes equation with the moving boundary. As mentioned in the Introduction, a simplified description of the recoiling motion has been very sparse. Especially, the closed form solution of the recoiling diameter of a high Oh droplet, Eq. (46), is the first in its kind to the authors' knowledge. In addition, by making use of the approximate models, an analytical study of the recoiling mechanism could be performed with great ease.

It is noteworthy that Pasandideh-Fard *et al.*[16] developed a composite model which assumes the spreading droplet shape to be a cylindrical disk under a truncated sphere (Fig. 11 therein). Our study shows that both the cylinder model and the truncated-sphere model have their own regimes where they are adequate, and this suggests that the composite model may turn out to be more generally applicable. However, it is difficult to come up with a simple parameter that defines the geometry of the shape as contrary to our current shape assumptions. Although a single parameter (either height or base diameter) is only necessary to define the shape of either a cylinder or a truncated sphere, the composite model requires more than one parameter including the base

diameter and the height of a cylindrical disk, to completely define the shape. Therefore, a single equation to describe the droplet motion such as Eq. (27) or (32) is not readily obtained in case of the composite model. Nevertheless, we expect that if a simple geometric parameter that can define the composite shape is derived, which is beyond the scope of this work, the composite model could yield more broadly applicable predictions.

It has been reported that when a droplet with a high surface tension collides with a relatively nonwettable solid surface, it tends to disengage from the surface upon hitting the surface. This total rebounding can be predicted by the truncated-sphere model and the corresponding results are shown in Bechtel *et al.*[20] However, the cylinder model is not adequate to accommodate total rebounding since as the base diameter gets very small, its height becomes so large as to satisfy the volume conservation. The resultant shape would be unrealistic to simulate the real droplet. Here we note that many computational programs solving the Navier–Stokes equation also have difficulties in modeling total rebounding since it involves a singular process of the droplet (computational domain) disengaging from the surface.

Our study shows that the recoiling behavior of water and ink droplets is determined by We, Oh, and the equilibrium contact angle. The Weber number determines the maximum spread diameter, which becomes the initial condition for the recoiling. The recoiling flow is driven by the capillarity force arising from the difference between the equilibrium state and the excessively spread shape. The flow is resisted by inertia and viscosity, and the resisting force is scaled by Oh. In the recoiling of the water droplets, whose Ohnesorge numbers are relatively small, both the inertia and the viscosity play significant roles in resisting the flow. Thus, the recoiling is vigorous and the cylinder model predicts the experimental results well. On the other hand, the recoiling of the ink droplets, whose Ohnesorge numbers are relatively large, is resisted dominantly by the viscosity. The ink droplets recoil relatively slowly and resemble a truncated sphere. Thus, the predictions of the truncated-sphere model agree with the experimental results fairly well. It has been shown that the recoiling is greatly affected by the wetting between the liquid droplet and the solid surface. Good wetting weakens and slows down the recoiling process, while poor wetting promotes the recoiling. The models incorporating the equilibrium contact angle in evaluating the potential energy term successfully predicted the dependence of the recoiling process on wetting.

ACKNOWLEDGMENTS

The authors are grateful to the Aluminum Company of America and to the National Science Foundation for the support of this work under Grant No. DMI-9634931.

APPENDIX A: NONDIMENSIONAL QUANTITIES

The following gives the definitions of the nondimensional quantities. Note that all the asterisked symbols denote dimensional quantities, whereas nonasterisked symbols are the corresponding nondimensional quantities except the material properties:

$$D_b=\frac{D_b^*}{D^*},\quad h=\frac{h^*}{D^*},\quad t=\frac{t^*}{(\rho D^{*3}/\sigma)^{1/2}},$$

$$T=\frac{T^*}{(\pi\sigma D^{*2}/12)},\quad V=\frac{V^*}{(\pi\sigma D^{*2}/12)},$$

$$v_z=\frac{v_z^*}{(\sigma/\rho D^*)^{1/2}},\quad v_r=\frac{v_r^*}{(\sigma/\rho D^*)^{1/2}},\quad z=\frac{z^*}{D^*},$$

$$\Delta_r=\frac{\Delta_r^*}{D^*},\quad \tau=\frac{\tau^*}{(\mu^2\sigma/\rho D^{*3})^{1/2}},\quad \Omega=\frac{\Omega^*}{(\pi D^{*3}/6)}.$$

APPENDIX B: DETERMINATION OF THE DISSIPATION FACTOR AND THE SENSITIVITY OF MODELING RESULTS TO ITS VALUES

The dissipation factor, F_d, has been introduced as an empirical constant in scaling the viscous stresses in the models above [Eqs. (13) and (39)]. Since our modeling of the viscous dissipation relies on the scaling analysis, the appropriate coefficients must be established by experiment or computation.[17] This is a common limitation of the order-of-magnitude analyses. Therefore, several studies to analytically model the viscous dissipation during droplet spreading have either assumed or empirically determined the coefficients. For example, Chandra and Avedisian[7] assumed the coefficients in their models of the viscous dissipation to be unity as seen in their Eqs. (13)–(15). Pasandideh-Fard *et al.*[16] also implicitly assumed the proportional constant in their modeling to be unity in their Eq. (9), which modeling turned out to be a fairly close approximation when compared with experimental results of the maximum spread factors. In addition, Bechtel *et al.*[20] included an adjustable proportional constant in modeling the shear stress at the droplet bottom as shown in their Eq. (17). Mao *et al.*[31] used a least-square method to deduce several constants appearing in their dissipation model [their Eq. (16)] based on their experimental results.

TABLE IV. Comparison of selected maximum spread factors of water droplets obtained by experiments ($D_{\max,\exp}$) and by model predictions ($D_{\max,\mathrm{cyl}}$ by the cylinder model). PW denotes present work.

We	Oh	$\theta(^\circ)$	$D_{\max,\exp}$	$D_{\max,\mathrm{cyl}}$	Reference
30	0.0017	87.4	2.27	2.59	PW
93.6	0.0020	67	3.09	3.38	Ref. 31
130	0.0020	37	3.70	3.79	Ref. 31
130	0.0020	67	3.67	3.58	Ref. 31
130	0.0020	97	3.60	3.42	Ref. 31
137	0.0017	87.4	3.16	3.58	PW
166	0.0019	58.6	3.71	3.84	PW
207	0.0018	87.4	3.91	3.85	PW
288	0.0020	37	4.50	4.31	Ref. 31
288	0.0020	67	4.42	4.17	Ref. 31
288	0.0020	97	4.32	4.02	Ref. 31
519	0.0020	97	4.78	4.52	Ref. 31
582	0.0017	87.4	5.13	4.75	PW

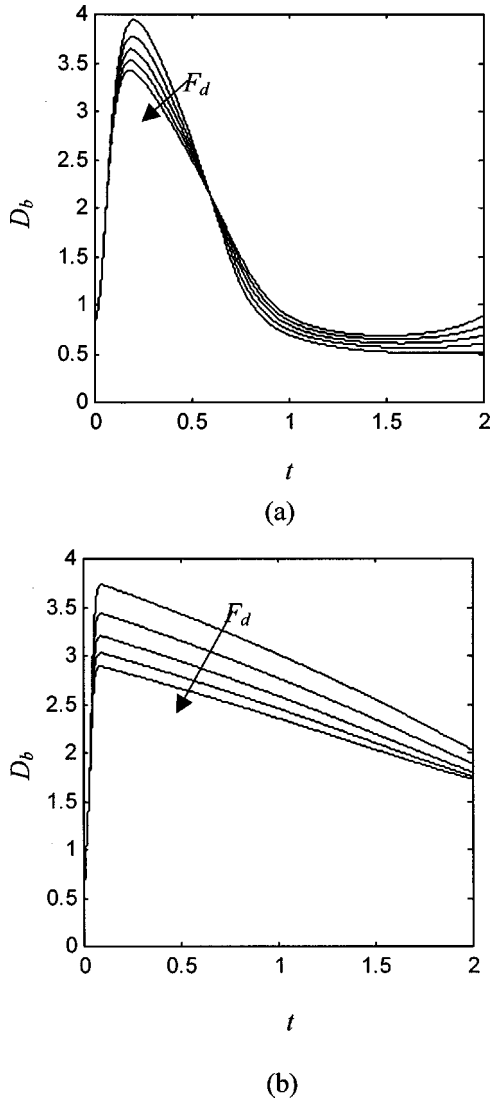

FIG. 18. Sensitivity of simulation results to the dissipation factor, F_d. (a) Water droplet on polycarbonate. We=150 and Oh=0.0017. Along the arrow, F_d=11, 13, 15, 17, and 19. (b) Ink droplet on polycarbonate. We=150 and Oh=0.006. Along the arrow, F_d=2.4, 2.8, 3.2, 3.6, and 4.0.

We determine the dissipation factors on an empirical basis, specifically by matching the maximum spread factors obtained by experiments conducted in this work. Moreover, for water droplets, we also used experimental results (maximum spread diameters) by Mao *et al.*[31] who reported the equilibrium contact angles with other impact conditions such as We and Oh. Based on the experimental results, the values of F_d, which best match $D_{\max}$ experimentally measured, are averaged. Table III shows the F_d values thus obtained, and Table IV shows selected experimental results for the maximum spread diameter used in this procedure along with model predictions, for water droplets.

Now we discuss the sensitivity of the modeling results to F_d. As F_d increases, both the maximum base diameter and the recoil speed decrease. The simulation results obtained by varying F_d in modeling a water droplet on polycarbonate and an ink droplet on polycarbonate are shown in Fig. 18. In the water droplet, whose dynamic conditions are typical ones in the experiments in this work, as F_d changes about $\pm 27\%$, the maximum base diameter and the recoil speed change approximately $\pm 8\%$ and $\pm 18\%$, respectively. In the ink droplet, as F_d changes about $\pm 25\%$, the maximum base diameter changes approximately -9% to $+15\%$, and the recoil speed changes approximately -4% to $+18\%$. Nevertheless, the general trend is invariant.

[1] A. M. Worthington, ''On the forms assumed by drops of liquid falling on a horizontal plate,'' Proc. R. Soc. London **25**, 26 (1877).
[2] A. M. Worthington, ''A second paper on the forms assumed by drops of liquid falling on a horizontal plate,'' Proc. R. Soc. London **25**, 498 (1877).
[3] O. G. Engel, ''Waterdrop collisions with solid surfaces,'' J. Res. Natl. Bur. Stand. **54**, 281 (1955).
[4] F. H. Harlow and J. P. Shannon, ''The splash of a liquid drop,'' J. Appl. Phys. **38**, 3855 (1967).
[5] C. D. Stow and M. G. Hadfield, ''An experimental investigation of fluid flow resulting from the impact of a water drop with an unyielding dry surface,'' Proc. R. Soc. London, Ser. A **373**, 419 (1981).
[6] K. Tsurutani, M. Yao, J. Senda, and H. Fujimoto, ''Numerical analysis of the deformation process of a droplet impinging upon a wall,'' JSME Int. J., Ser. II **33**, 555 (1990).
[7] S. Chandra and C. T. Avedisian, ''On the collision of a droplet with a solid surface,'' Proc. R. Soc. London, Ser. A **432**, 13 (1991).
[8] G. Trapaga and J. Szekely, ''Mathematical modeling of the isothermal impingement of liquid droplets in spraying processes,'' Metall. Trans. B **22**, 901 (1991).
[9] H.-H. Shi and J. P. Dear, ''Oblique high-speed liquid-solid impact,'' JSME Int. J., Ser. I **35**, 285 (1992).
[10] S. T. Thoroddsen and J. Sakakibara, ''Evolution of the fingering pattern of an impacting drop,'' Phys. Fluids **10**, 1359 (1998).
[11] H.-Y. Kim, Z. C. Feng, and J.-H. Chun, ''Instability of a liquid jet emerging from a droplet upon collision with a solid surface,'' Phys. Fluids **12**, 531 (2000).
[12] T. A. Elliott and D. M. Ford, ''Dynamic contact angles,'' J. Chem. Soc. **68**, 1814 (1972).
[13] L. Cheng, ''Dynamic spreading of drops impacting onto a solid surface,'' Ind. Eng. Chem. Process Des. Dev. **16**, 192 (1977).
[14] J. Fukai, Y. Shiiba, T. Yamamoto, O. Miyatake, D. Poulikakos, C. M. Megaridis, and Z. Zhao, ''Wetting effects on the spreading of a liquid droplet colliding with a flat surface: Experiment and modeling,'' Phys. Fluids **7**, 236 (1995).
[15] J. Fukai, Y. Shiiba, and O. Miyatake, ''Theoretical study of droplet impingement on a solid surface below the Leidenfrost temperature,'' Int. J. Heat Mass Transf. **40**, 2490 (1997).
[16] M. Pasandideh-Fard, S. Qiao, S. Chandra, and J. Mostaghimi, ''Capillary effects during droplet impact on a solid surface,'' Phys. Fluids **8**, 650 (1996).
[17] S. Schiaffino and A. A. Sonin, ''Molten droplet deposition and solidification at low Weber numbers,'' Phys. Fluids **9**, 3172 (1997).
[18] S. D. Aziz and S. Chandra, ''Impact, recoil and splashing of molten metal droplets,'' Int. J. Heat Mass Transf. **43**, 2841 (2000).
[19] G. E. Kendall and W. M. Rohsenow, ''Heat transfer to impacting drops and post critical heat flux dispersed flow,'' Technical Report No. 85694-100, Dept. Mechanical Eng., MIT, Cambridge, MA, 1978.
[20] S. E. Bechtel, D. B. Bogy, and F. E. Talke, ''Impact of liquid drop against a flat surface,'' IBM J. Res. Dev. **25**, 963 (1981).
[21] J. Madejski, ''Solidification of droplets on a cold surface,'' Int. J. Heat Mass Transf. **19**, 1009 (1976).
[22] H. Fukanuma, ''A porosity formation and flattening model of an impinging molten particle in thermal spray coatings,'' J. Thermal Spray Tech. **3**, 33 (1994).
[23] A. A. Korobkin, ''Asymptotic theory of liquid–solid impact,'' Philos. Trans. R. Soc. London, Ser. A **355**, 507 (1997).
[24] J.-Y. Lai (private communication).
[25] S. Schiaffino, ''The fundamentals of molten microdrop deposition and solidification,'' Ph.D. thesis, MIT, Cambridge, MA, 1996.
[26] S. H. Crandall, D. C. Karnopp, E. F. Kurtz, Jr., and D. C. Pridmore-Brown, *Dynamics of Mechanical and Electromechanical Systems* (McGraw-Hill, New York, 1968).
[27] L. H. J. Wachters and N. A. J. Westerling, ''The heat transfer from a hot

wall to impinging water drops in the spheroidal state,'' Chem. Eng. Sci. **21**, 1047 (1966).
[28]G. B. Foote, ''The water drop rebound problem: Dynamics of collision,'' J. Atmos. Sci. **32**, 390 (1975).
[29]R. E. Ford and C. G. L. Furmidge, ''Impact and spreading of spray drops on foliar surfaces,'' Wetting, Soc. Chem. Ind., Monograph **25**, 417 (1967).
[30]V. P. Carey, *Liquid-Vapor Phase-Change Phenomena* (Hemisphere, Washington, 1992).
[31]T. Mao, D. C. S. Kuhn, and H. Tran, ''Spread and rebound of liquid droplets upon impact on flat surfaces,'' AIChE J. **43**, 2169 (1997).
[32]G. K. Batchelor, *An Introduction to Fluid Dynamics* (Cambridge University Press, Cambridge, England, 1967), p. 354.
[33]X. Zhang and O. A. Basaran, ''Dynamic surface tension effects in impact of a drop with a solid surface,'' J. Colloid Interface Sci. **187**, 166 (1997).
[34]D. Richard and D. Quéré, ''Viscous drops rolling on a tilted non-wettable solid,'' Europhys. Lett. **48**, 286 (1999).
[35]R. F. Allen, ''The role of surface tension in splashing,'' J. Colloid Interface Sci. **51**, 350 (1975).